Title

Phosphoinositide 3-kinase regulates the role of retromer in transcytosis of the polymeric immunoglobulin receptor

Journal

Experimental Cell Research, 313(4)

ISSN

0014-4827

Authors

Vergés, Marcel
Sebastián, Isabel
Mostov, Keith E

Publication Date

2007-02-01

DOI

10.1016/j.yexcr.2006.11.010

PHOSPHOINOSITIDE 3-KINASE REGULATES THE ROLE OF RETROMER IN TRANSCYTOSIS OF THE POLYMERIC IMMUNOGLOBULIN RECEPTOR

Marcel Vergés[1,2], Isabel Sebastián[2] and Keith E. Mostov[1]

[1]Department of Anatomy, Cardiovascular Research Institute and Department of Biochemistry and Biophysics, University of California School of Medicine, San Francisco, California 94143-2140, USA; [2]Laboratory of Epithelial Cell Biology, Centro de Investigación Príncipe Felipe, 46013 Valencia, Spain.

Address for manuscript correspondence:

Marcel Vergés, Laboratory of Epithelial Cell Biology, Centro de Investigación Príncipe Felipe, 46013 Valencia, Spain; Tel +34 96 328 9680; Fax +34 96 328 9701; E-mail: mverges@cipf.es

Abstract

Retromer is a multimeric protein complex that mediates intracellular receptor sorting. One of the roles of retromer is to promote transcytosis of the polymeric immunoglobulin receptor (pIgR) and its ligand polymeric immunoglobulin A (pIgA) in polarized epithelial cells. In Madin-Darby Canine Kidney (MDCK) cells, overexpression of Vps35, the retromer subunit key for cargo recognition, restores transcytosis to a pIgR mutant that is normally degraded. Here we show that pIgA transcytosis was not restored in these cells when treated with the specific phosphoinositide 3-kinase (PI3K) inhibitor LY294002. Likewise, the decrease in pIgA transcytosis by wild-type pIgR seen upon PI3K inhibition was not reverted by Vps35 overexpression. PI3K inhibition reduced membrane association of sorting-nexins (SNX) 1 and 2, which constitute the retromer subcomplex involved in membrane deformation, while association of the Vps35-Vps26-Vps29 subcomplex, involved in cargo recognition, remained virtually unaffected. Colocalization between the two retromer subcomplexes was reduced upon the treatment. Whereas the interaction among the subunits of the Vps35-Vps26-Vps29 subcomplex remained unchanged, less Vps35 was found associated with pIgR upon PI3K inhibition. In addition, colocalization of internalized pIgA with subunits of both retromer subcomplexes throughout the transcytotic pathway was substantially reduced by LY294002 treatment. These data implicate PI3K in controlling retromer's role in pIgR-pIgA transcytosis.

Keywords: MDCK, receptor, pIgR, transcytosis, retromer, Vps35, sorting-nexin, phosphoinositide, phosphatidylinositol, LY294002

Introduction

Epithelial cells have apical and basolateral plasma membrane domains that are morphologically and functionally differentiated and separated by specialized cell-cell junctions. A highly organized membrane traffic network allows proper distinction of these plasma membrane domains [1]. Newly synthesized plasma membrane proteins are first sorted in the *trans*-Golgi network for delivery to the apical or basolateral surface. Proteins can then be endocytosed from one surface and recycled back to that surface, be degraded in the lysosomes, or transcytosed to the opposite cell surface. As the cell has to transport cargo selectively by transcytosis across two different environments, proper sorting of proteins along this pathway is essential for maintaining cell polarity [2]. Transcytosis of the polymeric immunoglobulin receptor (pIgR), which transports polymeric immunoglobulin A (pIgA) across epithelia, has been extensively studied in hepatocytes, enterocytes and Madin-Darby Canine Kidney (MDCK) cells stably expressing pIgR. In these cell types, pIgR binds pIgA at the basolateral plasma membrane and is transcytosed through various intracellular intermediates to the apical surface. Once at the apical plasma membrane, the ligand-binding portion of pIgR is cleaved off and released together with the ligand into the apical lumen, where it will perform antigen exclusion [2, 3].

Receptor sorting at the endosomal compartment is thought to be mediated by interactions of the receptor's cytosolic domain with peripheral membrane proteins or protein complexes. A remarkable example of these sorting events is performed by a multimeric protein complex termed retromer. In analogy to its role first proposed in yeast [4, 5], retromer performs endosome-to-Golgi retrieval of the cation-independent mannose 6-phosphate receptor (CI-MPR) in mammalian cells, once delivery of lysosomal hydrolases by the receptor has been completed [6-8]. We previously found that retromer also associates with

pIgR and promotes transcytosis of pIgR-pIgA in polarized MDCK cells. This led us to the hypothesis that retromer could be performing an analogous role in this system as for CI-MPR retrieval, preventing missorting to lysosomes and degradation of pIgR-pIgA [9]. The recent understanding of retromer's involvement in protein trafficking in multicellular organisms has led to the proposal that there are multiple recycling or retrieval pathways for endosomal cargo (reviewed in [8, 10])

Based on early studies in the yeast model, retromer assembly and functioning involves the cooperation of two subcomplexes. One subcomplex consists of two sorting-nexins (SNXs), Vps5p and Vps17p, which self-assemble and cooperate for membrane deformation and coat formation [4, 11, 12]. The second subcomplex consists of Vps35p, Vps29p and Vps26p. Of these subunits, Vps35p provides cargo specificity and associates directly with cargo proteins [13, 14]; Vps29p serves a catalytic role, activating Vps35p and promoting its oligomerization [4, 5]; and Vps26p promotes or stabilizes the interaction between the SNXs subcomplex and the cargo-selective Vps35p, and may also contribute to Vps35p membrane association [15]. There is evidence that retromer assembles in a similar way in higher eukaryotes, with Vps35 serving as the platform for complex formation [16, 17]. Vps35 also associates directly with cargo in mammalian systems [6]. Indeed, recent data from structural and binding studies has provided valuable information on the protein-protein interaction sites among retromer subunits and on how the subunits are integrated within the retromer complex [17-19]. However, important aspects on regulation of retromer at a cellular level remain to be carefully studied. That is, what regulates retromer's assembly and association to membranes, and how these processes affect retromer's sorting function? In yeast, retromer's recruitment and activation require phosphoinositide 3-kinase (PI3K) activity and formation of a specific pool of phosphatidylinositol (PI) 3- phosphate [20]; a similar role for PI lipids in ensuring proper membrane association of retromer has also been proposed in mammalian cells [6, 21].

These data, as well as previous work implicating the PI3K pathway on pIgR transcytosis [22, 23], prompted us to analyze the regulation of retromer's role in pIgR-pIgA transcytosis by PI3K.

Materials and Methods

Cell culture, transfection, adenoviral infection and treatment with LY294002 – Polarized MDCK II cells and transfectant derivates were maintained in MEM 10 % FBS, including Earle's salts, L-Gln and L-Met. Unless otherwise specified, cells were grown on Transwell polycarbonate filters of 12 mm diameter and 0.4 μm pore size (Corning-Costar, Cambridge, MA). The cell line stably expressing wild-type pIgR (pIgR-WT) and the tetracycline transactivator (tTA) [24], also available from Clontech Laboratories (Palo Alto, CA), and the cell line expressing the mutant pIgR$^{\Delta 670\text{-}707}$ [25] have been reported.

The 5'-myc-tagged cDNA constructs for expression of full-length human SNX2 and Vps35 have been described [16]. For transfection, MDCK pIgR-WT cells [26] were plated on 12-well plates at 150,000 cells / well and transfected after 24 h with 1 μg DNA construct using Lipofectamine 2000 reagent (Invitrogen, Carlsbad, CA) according to the manufacturer's instructions. For stable expression of myc-hSNX2, cells were transfected and grown in selective medium containing 0.7 mg / ml Geneticin (G418) sulfate (Invitrogen). Positive clones were screened for myc-SNX2 expression by western blot and immunofluorescence, and the proper distribution of cell surface markers was analyzed as previously described [9].

Recombinant adenoviruses encoding myc-hVps35 or the tTA were produced previously and infections were performed under a tetracycline repressible system as described [9]. As quantitated from western blots, lysates of cells induced for 16 h in the absence of

doxycycline show ≥ 5-fold Vps35 overexpression over those of control cells (repressed with the antibiotic).

LY294002 was purchased from Sigma-Aldrich (St. Louis, MI), dissolved at 25 mM in DMSO as a stock and stored at –20^{o}C. Incubations were for 30 min at the indicated concentration. An equivalent volume of the solvent was added in the cell culture media of untreated cells. In experiments involving internalization of pIgA (radiolabeled or not), the inhibitor was kept throughout a 10 min pulse with basolateral pIgA and during chase in ligand-free medium.

Antibodies – Rabbit polyclonal antibodies anti-human Vps35, Vps26, Vps29, SNX1, and SNX2 have been described [16]. Antibodies against pIgR were a sheep polyclonal to the receptor's secretory component (prepared by us), and a mouse monoclonal to the receptor's cytoplasmic tail, SC166 (a gift from J-P Kraehenbuhl, ISREC, Lausanne, Switzerland). Human pIgA was provided by J-P Vaerman (UCL, Brussels, Belgium). Other primary antibodies used are commercially available. These were a rabbit polyclonal against Akt phosphorylated at Ser473 (P-AKT) (Cell Signaling Technology, Beverly, MA), a mouse monoclonal against early endosome antigen 1 (EEA1) (Transduction Laboratories, Lexington, KY), a mouse monoclonal to actin (Boehringer Mannheim, Indianapolis, IN), and a mouse anti-myc tag monoclonal generated from 9E10 hybridoma (ATCC, Manassas, VA). Secondary antibodies HRP-conjugated for western blot, and the secondary to human IgA TRITC-conjugated for immunofluorescence, were from Jackson ImmunoResearch Laboratories (West Grove, PA); Alexa-conjugated antibodies for immunofluorescence were from Molecular Probes (Eugene, OR).

Isolation of membrane and cytosol fractions – All steps were done at 4^{o}C. MDCK cells were grown to confluence on 6 cm plates and scrapped in 1 ml homogenization buffer, which contained 10 mM triethanolamine, 8.24 % sucrose, 1 mM EDTA, 10 mM NaF, 1 mM

Na_3VO_4 and a cocktail of protease inhibitors (0.4 mM AEBSF, 307 nM aprotinin, 10.5 µM leupeptin, 2.8 µM E64 and 3.19 mM benzamidine). The cell suspension was left on ice for 15 min, transferred into a 2 ml Teflon-glass homogenizer and thoroughly homogenized (25 strokes); trypan blue staining confirmed > 70 % cell breakage. The homogenate was spun 5 min at 1,000 g to obtain a post-nuclear supernatant. The supernatant was transferred into a microfuge polyallomer tube and spun at 125,000 g_{av} for 1h in a Beckman TLA-55 fixed angle rotor, to separate a membrane pellet (resuspended in 50 µl 1 % SDS – H_2O) from the soluble cytosolic fraction. Starting from ~ 2 mg homogenate protein, ~ 250 µg membrane protein and ~ 700 µg cytosol protein were obtained.

Co-immunoprecipitation and western blot analysis – All steps were done at 4°C. Immunoprecipitation of pIgR was performed using the sheep polyclonal antibody as described [9]. Slight modifications were done to immunoprecipitate retromer. Briefly, MDCK cells were grown to confluence on 6 or 10 cm dishes and lysed in ~ 40 µl Lysis Buffer (0.5 % NP-40, 20 mM Tris at pH 7.4, 100 mM NaCl, 0.5 mM EDTA, and protease inhibitors as above) / cm^2 of plate surface. Each immunoprecipitation was performed with ~ 0.75 mg protein (0.5 ml lysate), after clearing the lysate by centrifugation for 15 min at 16,000 g. The supernatant was transferred to a tube containing 10 µl protein A-Sepharose beads coupled to the anti- Vps26 antibody (~ 5 µg IgG per sample) and immunoprecipitated for 1 h. In some experiments, the antibody was chemically cross-linked to the beads with dimethyl pimelimidate (Pierce Biotechnology, Rockford, IL). Beads were pelleted, washed 3 X in Lysis Buffer, once in Lysis Buffer without NP-40, and processed for western blot. The degree of association between proteins was calculated as described [9].

Protein concentration of samples for SDS-PAGE and western blotting analysis was determined by the bicinchoninic acid assay (Pierce). Protein bands were visualized by

enhanced chemiluminescence in an ImageQuant ECL imager and band intensities quantitated using the ImageQuant TL software (GE Healthcare Bio-sciences, Piscataway, NJ).

Internalization of pIgA, immunofluorescence and confocal microscopy analysis – Uptake of human pIgA, processing of cells for immunofluorescence and image analysis were performed essentially as described [9]. Images were taken in a Leica TCS-SP2-AOBS confocal microscope. Measurements of endosomal size were performed using the Leica Confocal Software (LCS). For each treatment, four representative areas were taken at high magnification and a total of ~ 350 endosomes per treatment were analyzed. The LCS was also used to determine percentage of protein colocalization. To quantitate colocalization between pIgA and retromer, we analyzed 80-100 structures loaded with internalized pIgA from two pictures of each representative plane of the cell, subapical (at the level of tight junctions), at the nucleus level, and basolateral. The relative presence of a retromer subunit in each of these pIgA-positive structures was evaluated by calculating the ratio of mean energy units / pixel between each fluorescence channel and plotting this value as percentage of colocalization. We considered SNX2 as representative of the SNXs and Vps26 as representative of the Vps35-Vps26-Vps29 retromer subcomplex since immunofluorescence staining using the corresponding antibodies displayed well-defined vesicular patterns. To quantitate colocalization between subunits of the two retromer subcomplexes, an analogous procedure was followed by analyzing 80-100 structures positive for myc-hSNX2 and determining the relative presence of Vps26 in each of these structures.

Transcytosis assay – The assay for ^{125}I-pIgA transcytosis has been previously described [27]. Calculated from the total radioactivity incorporated in each sample, the data was plotted as percentage of ligand apically delivered, basolaterally recycled or degraded, the latter, equivalent to the counts remaining in the supernatant after TCA precipitation.

Results

PI3K inhibition reduces pIgR-pIgA transcytosis even if the pathway is promoted by Vps35 overexpression – We previously found that the Vps35-Vps26-Vps29 retromer subcomplex associates with pIgR and promotes transcytosis of pIgR-pIgA in polarized MDCK cells [9]. To investigate whether PI3K controls the retromer's role in pIgR-pIgA trafficking, we tested the effect on pIgA transcytosis of the specific PI3K inhibitor LY294002 [28]. We first determined the smallest dose of the inhibitor that will abrogate appreciable PI3K activity by analyzing the effect of various concentrations of LY294002 on dephosphorylation of protein kinase B (PKB/Akt), a major downstream PI3K target [29]. As quantitated from western blots using an anti-P-AKT antibody, 30 min incubation with 10 μM LY294002 was sufficient to decrease cytosolic Akt phosphorylation by 86 %, and virtually no P-Akt was left at 50 μM (99 % reduced) and beyond (Fig. 1a). To evaluate such effect at the level of intracellular membranes, we also analyzed membrane depletion of EEA1, a well-known Rab5 effector whose association with endosomes requires PI3K activity [30]. Concentrations of inhibitor at 10 μM or lower did not markedly affect EEA1 association with membranes (not shown). However, incubations at 20, 50 and 100 μM LY294002 for 30 min depleted EEA1 from membranes by 45, 59 and 80 %, respectively (Fig. 1b, upper panel). Actin, used as a loading control, remained in a constant cytosol / membrane ratio under all concentrations used (Fig. 1b, lower panel). Incubation with LY294002 for longer than 30 min did not result in further inhibition, as measured by either cytosolic AKT dephosphorylation or EEA1 membrane depletion (data not shown). We therefore chose this period of incubation for all experiments.

PI3K inhibitors have been shown to increase endosome size [31], probably by affecting membrane trafficking from endosomes [32] and by inhibiting inward vesiculation

for multivesicular body formation [33]. On the other hand, EEA1 depleted endosomes are unable to fuse *in vitro* [34]. To evaluate these effects in our system, we measured the size of EEA1 immunostained endosomes in cells treated with different concentrations of LY294002. In spite of the redistribution to cytosol seen by western blot (Fig. 1b), EEA1 vesicular staining was not seen dramatically affected under the various concentrations of inhibitor tested (Fig. 2a). However, with 100 μM LY294002, less and larger EEA1 labeled endosomes were observed (arrowheads), some of them appearing blurry (asterisks), perhaps as a result of the loss of this endosomal marker from membranes as well as to a redistribution to certain endosome subdomains (Fig. 2a). At 10 μM, EEA1 positive endosomes increased their diameter by only 4 % in average (n ~ 350; $p = 0.01$). Up to 50 μM, this percentage did not consistently go up, but we measured an average 70 % increase in size at 100 μM ($p < 0.0001$), the highest concentration tested (Fig. 2b). This morphologic analysis indicates that general effects on endosome dynamics were minimal under the protocol that we used to inhibit PI3K, although such effects could become significant at high concentrations of the inhibitor. We therefore performed a dose-response experiment to determine the effect on pIgA transcytosis testing a low (10 μM) and a moderate (50 μM) concentration of the inhibitor; we found practically no effect with 10 μM, but transcytosis went from 69 % down to 57 % with 50 μM LY294002 after a 60 min chase (Fig 3a). A parallel increase of basolaterally recycled (from 9 % to 13 %; not shown) and degraded ligand (from 10 % to 17 %; Fig 3a) was also measured throughout this period of time. This inhibitory tendency agrees with previously published data showing that wortmannin, another commonly used PI3K inhibitor, inhibits pIgA transcytosis [22, 23].

We have shown that transient overexpression of myc-hVps35 in MDCK cells by adenovirus-mediated gene transfer under a tetracycline repressible system increases pIgR-pIgA transcytosis [9]. We then tested the effect of PI3K inhibition on pIgA transcytosis in

adenovirus-induced cells. Here, the decrease of ligand transcytosis was somewhat lower, albeit apparent, going from 73 % down to 65 % when using the inhibitor at 50 μM (Fig. 3b). Although ligand recycling barely changed (it went from 7 % to 9 %; not shown), degradation still increased noticeably (from 10 % to 15 %; Fig. 3b). Thus, Vps35 overexpression only partially prevented LY294002 inhibition of pIgA transcytosis, indicating that overexpressed Vps35 cannot bypass the requirement of PI3K activity.

Transcytosis of pIgA by pIgR$^{\Delta 670\text{-}707}$ is not restored by Vps35 overexpression when PI3K is inhibited – In MDCK cells expressing a pIgR mutant with an internal deletion in its cytoplasmic tail (MDCK-pIgR$^{\Delta 670\text{-}707}$), most of pIgA is degraded and less than 5 % is transcytosed [25]. In these cells, 50 μM LY294002 reduced ligand degradation from 76 % down to 47 % (Fig 4c), likely a result of affected lysosomal function, as described [32, 35, 36]. The endocytosis rate was unchanged (not shown) and transcytosis remained almost undetectable (Fig 4a). However, basolateral recycling went up from 9 % to 38 % in treated cells (Fig 4b), suggesting that PI3K is not necessary for pIgA recycling or that PI3K inhibits recycling.

We have shown that Vps35 overexpression markedly increases transcytosis in MDCK-pIgR$^{\Delta 670\text{-}707}$ cells [9]. Similarly, we show here that pIgA transcytosis goes from ~ 0 % up to 24 % upon Vps35 overexpression (Fig. 4a). Strikingly, PI3K inhibition reduced this positive effect, leaving the percentage of transcytosed ligand at 2 %, i.e. resembling that in uninduced control cells (Fig. 4a). While ligand degradation remained almost unchanged when inhibiting PI3K (Fig 4c), basolateral recycling still went up from 11 % to 26 % (Fig 4b), and this difference mostly accounted for the sharp reduction observed in apical delivery. These data, along with the assays above using pIgR-WT, implicate PI3K in the regulation of retromer's role in pIgA transcytosis.

Membrane association and assembly of the retromer subcomplexes is regulated independently – Our interpretation of these results is that decrease of PI 3-phosphates by PI3K inhibition reduces the efficiency of SNXs association to membranes, and hence of retromer assembly [6, 20, 21], thereby affecting retromer's role in pIgR-pIgA transcytosis. We tested this directly by analyzing a possible redistribution of retromer subunits to the cytosol caused by PI3K inhibition (Fig. 5a). Quantitation of western blots indicates a clear tendency of SNXs depletion from membranes in the presence of LY294002. However, none of the subunits of the Vps35-Vps26-Vps29 subcomplex showed a marked decrease in membrane association, perhaps with the exception of Vps35, which levels changed slightly (Fig. 5b). Nevertheless, the differences found in Vps35 levels were not statistically significant under the various concentrations of the inhibitor tested (p = 0.40 and p = 0.44, respectively, for 50 μM and 100 μM LY294002 vs. the untreated control; n = 4). Thus, while SNXs association to membranes was affected by PI3K inhibition, association and supposedly assembly of the Vps35-Vps26-Vps29 subcomplex was not.

To address the interaction *in vivo* among these subunits, we attempted to immunoprecipitate the retromer complex. As quantitated from western blots, 29 % Vps35 and 77 % Vps29 were found complexed with Vps26, indicative of a tight association among the subunits of the Vps35-Vps26-Vps29 subcomplex. However, SNX1 or SNX2 were not detected in these immunoprecipitates (Fig. 6a), may be as a consequence of weak or transient interactions between the two subcomplexes. To analyze a possible involvement of PI3K in establishing or maintaining these interactions, we compared the relative association among retromer subunits in cells treated with 50 μM LY294002 with that in untreated cells. No differences were found in the stoichiometry of the interactions among the subunits of the Vps35-Vps26-Vps29 subcomplex (Fig. 6b). Vps35 overexpression had no effect on these associations, and in all cases both SNX1 and SNX2 remained undetected in the

immunoprecipitates (not shown). Altogether, these data emphasize the idea that membrane association and assembly of the two retromer subcomplexes undergo an independent regulation. Thus, a complete association of both subcomplexes to the membrane is not required for assembly of the Vps35-Vps26-Vps29 subcomplex, but appears necessary for efficient cargo sorting.

PI3K inhibition alters the association between the two retromer subcomplexes and between retromer and cargo – Inhibition of PI3K by LY294002 differentially affected membrane association of the SNXs and the Vps35-Vps26-Vps29 subcomplex (Fig. 5). It seems therefore possible that the lack of PI 3-phosphates actually prevents association of retromer onto appropriate endosome locations. To study this possibility, we used MDCK cells stably expressing myc-hSNX2 and analyzed if colocalization between the two retromer subcomplexes at representative cell sections was affected upon PI3K inhibition (see Methods for details). We first verified a proper subcellular location of the exogenous protein. As quantitated from immunofluorescence images, myc-hSNX2 displayed ~ 70 % overlap with total SNX2 throughout the cell, being the colocalization more apparent at the subapical region (not shown). We also observed that myc-SNX2 markedly colocalized with endogenous Vps26, suggesting a correct integration in the retromer complex (Fig. 7). When cells were treated with 50 μM LY294002, we found a significant decrease in the colocalization between myc-SNX2 and Vps26, particularly manifested at the subapical region of the cell (Fig. 7a), but also apparent at the nuclear region (Fig. 7b). This reduced colocalization between the two retromer subcomplexes prompted us to analyze if, as a consequence, PI3K inhibition altered colocalization between internalized pIgA and retromer. Consistent with previous data [9], we found that pIgA partially colocalized with Vps26 (Fig. 8). While particularly evident at the region around the nucleus (Fig. 8a), we found a significant decrease of colocalization between pIgA and Vps26 in the presence of the inhibitor throughout the cell. Such decrease was

already quantifiable with 10 μM (not shown), but it was more manifested with 50 μM LY294002 (Fig. 8b). Upon overexpression of Vps35, which promotes the pIgR transcytotic pathway [9], a slight increase in Vps26 colocalization with pIgA was measured in untreated cells. However, we still found a considerable loss of colocalization by the treatment, except at the subapical region, for which differences were not statistically significant (Fig. 8c). In agreement with this altered colocalization between internalized pIgA and Vps26, we found that less Vps35 co-immunoprecipitated with the pIgR in cells treated with the inhibitor; this association was reduced by the treatment from 1.73 % down to 0.66 % (Fig. 6c). We also analyzed colocalization between pIgA and SNX2. Here, the decrease of colocalization caused by LY294002 treatment was obvious at the subapical (Fig. 9a) and basolateral regions of the cell (Fig. 9b), perhaps owed to a large proportion of cytosolic SNX2 displaying a diffuse pattern at the perinuclear area (not shown), which may have overestimated our measurements in this region. Upon Vps35 overexpression, a general decrease in pIgA-SNX2 colocalization was also observed when inhibiting PI3K (Fig. 9c). Decrease in colocalization with Vps26 (Supplemental Fig. 1) and with SNX2 (Supplemental Fig. 2) was still observed when internalized pIgA was chased for long time periods (up to 30 min), during which the ligand gradually leaves basolateral endosomes but it is still detected at the subapical cell region [37]. In summary, the reduced colocalization observed between the two retromer subcomplexes and between retromer and cargo provides an explanation for the effects of PI3K inhibition on pIgA transcytosis.

Discussion

In this study we present evidence that PI3K regulates the retromer's role in transcytotic delivery of pIgR-pIgA through polarized MDCK cells. Our conclusion is strongly

supported by the consequences of specifically inhibiting PI3K with LY294002 in MDCK-pIgR$^{\Delta 670\text{-}707}$ cells, which are defective in pIgA transport [25]. In these cells, Vps35 overexpression promotes transcytosis of an otherwise quickly degraded ligand [9]. Here, PI3K inhibition dramatically reduced the restored transcytosis accomplished by Vps35 overexpression (Fig. 4a).

In the present work, it was critical to distinguish whether possible effects measured on pIgA transcytosis were specific of regulation by PI3K-retromer and did not occur owed to more general alterations throughout the endocytic-transcytotic pathway inherent of the approach used. To study PI3K regulation of retromer's function, we chose a chemical approach to specifically block the enzyme's activity. The enzyme's inhibitor, its concentration as well as exposure time were carefully established. We evaluated inhibition of Akt phosphorylation [29], EEA1 depletion from membranes [30] and endosome enlargement [31, 32]. Based on these analysis (Fig. 1 and Fig. 2), we chose 10 μM and 50 μM, respectively, as low and intermediate (moderate) concentrations of LY294002 to use for functional assays (Fig. 3 and Fig. 4). At 50 μM, LY294002 has been reported to display a very specific effect, without affecting a representative range of tyrosine kinases, serine-threonine kinases, lipid kinases, or ATPases [28]. More recently, however, it was shown that PI3K inhibitors could also inhibit kinases with a catalytic domain similar to that of PI3K. In this regard, LY294002 appeared to inhibit the mammalian target of rapamycin at only 30 μM [38]. Such additional inhibitory effect may have long-term implications on cell proliferation and further consequences in various systems, but it is unlikely that interferes with IgA trafficking as measured in our short-term analysis. Another kinase reported to display sensitivity for LY294002 is casein kinase II (CK2). As reported, 50 μM LY294002 nearly inhibited CK2 to a similar extent as PI3K [39]. Among many potential substrates, CK2 phosphorylates proteins that traffic between intracellular compartments and the plasma

membrane, including endosomal receptors; a putative CK2 phosphorylation site has also been proposed for pIgR at Ser^{726}, however, *in vitro* or *in vivo* evidence of CK2 phosphorylation on pIgR was not provided [40]. Even if we inhibited CK2 dependent phosphorylation of pIgR in our experiments, phosphorylated Ser^{726} appears to be required for interaction of pIgR with the AP-1 clathrin adaptor at the *trans*-Golgi network and to function on pIgR targeting to the basolateral surface [40]. On the contrary, we have measured basolateral to apical transcytosis of pIgA, and expressed this as a percentage, which is independent of pIgR expression levels and of receptor levels on the basolateral surface [27]. Thus, although we cannot completely rule out effects on other enzymes by LY294002 under our experimental conditions, such effects unlikely had implications in our assays of pIgA transcytosis.

Transcytosis of pIgA decreased with 50 μM LY294002 (Fig. 3a). This decrease was moderate in comparison to the 50 % inhibition previously reported under wortmannin [22], although the effects on pIgA transcytosis could largely depend on the inhibitor and dose used [23]. It should be noted that the two inhibitors present important differences, which turn into an IC_{50} ~ 500-fold lower for wortmannin than for LY294002 [41]. It is possible that the concentration of wortmannin used to inhibit PI3K in these studies was disproportional in comparison to the concentration of LY294002 that we have used here, and the more striking effect that was then seen on transcytosis might have been caused by broad effects on the endosomal machinery, as discussed above [31, 32, 34]. On the other hand, the lack of a striking effect on pIgA transcytosed by pIgR-WT (Fig. 3) suggests that the effects seen on pIgA transcytosed by $pIgR^{\Delta 670\text{-}707}$ (Fig. 4) are specific to PI3K inhibition and unrelated to possible side effects on membrane dynamics or to inhibition of other kinases putatively involved in pIgR trafficking.

Retromer ensures efficient transcytosis of pIgA by pIgR-WT or $pIgR^{\Delta 670\text{-}707}$ and prevents their degradation [9]. In the present work, PI3K inhibition markedly increased

basolateral recycling of pIgA by pIgR$^{\Delta 670\text{-}707}$. In MDCK-pIgR$^{\Delta 670\text{-}707}$ cells overexpressing Vps35, PI3K inhibition blocked the ability of retromer to restore pIgA transcytosis, without affecting further ligand degradation, while recycling still increased (Fig. 4). These observations fit with a model in which PI3K would act in a post-endocytic, intermediate step of transcytosis, prior to translocation of pIgR-pIgA into an apical compartment, as previously proposed [22]. The present data suggest that retromer regulation by PI3K would prevent ligand recycling rather than ligand degradation, perhaps as a result of promoting its transcytosis, in agreement to what we previously proposed [9].

We assume that the concentration dependency of EEA1 dissociation that we found in response to LY294002 parallels a decrease in endogenous PI 3-phosphates, as previously observed to occur in response to wortmannin [30, 42]. An interpretation of our data is that such decrease in PI 3-phosphates prevents SNXs association to membranes [6, 21] and hence retromer assembly [20], thus affecting retromer activity on pIgR-pIgA transcytosis. Although there is compelling evidence for a role of PI 3-phosphates on recruitment of SNXs through their Phox homology (PX) domain (reviewed in [43-45]), this aspect still remains a matter of controversy. In this regard, deletion of Vps34p, the only PI3K in yeast [46], or deletion of the PX domain of either Vps5p or Vps17p, only caused a modest effect on Vps5p membrane association [11]. In mammalian systems, SNX1 was proposed to associate with the Vps35-Vps26-Vps29 subcomplex [16] and to be preferentially targeted, through its Bin/Amphiphysin/Rvs and PX domains, to tubular endosome microdomains rich in PI 3-phosphates [47]. According to the model proposed, SNX1 acts as a scaffold for association of the Vps35-Vps26-Vps29 subcomplex, which then selects cargo for sorting by an iterative fractionation process based on the geometric efficiency of these tubular elements [47]. However, we have not found SNX1 or the closely related SNX2 associated with pIgR-WT [9] or present in co-immunoprecipitated Vps35-Vps26-Vps29 subcomplexes. In addition,

inhibition of PI3K did not affect the stoichiometry of the interactions among these subunits (Fig. 6). This suggests that SNXs association to the Vps35-Vps26-Vps29 subcomplex may be transient and that assembly of the two subcomplexes undergoes independent regulation. In agreement with these data, SNX1 has not been detected in pull-down assays of mammalian Vps29 [17] and antisense depletion of both SNX1 and SNX2 did not prevent targeting of Vps26 to membranes [48]. In a reciprocal way, knocking down Vps35 [9] or Vps26 [6, 7, 49] depletes the Vps35-Vps26-Vps29 subcomplex but does not affect the levels of SNX1 or SNX2. Similarly, SNXs displayed a clear tendency of redistribution to cytosol upon PI3K inhibition under our experimental conditions, leaving the subunits of the Vps35-Vps26-Vps29 subcomplex largely unaffected (Fig. 5). We propose that this redistribution is responsible for the altered colocalization between exogenous SNX2 and endogenous Vps26 observed upon PI3K inhibition (Fig. 7), and for the consequent reduction in Vps35 co-immunoprecipitated with pIgR (Fig. 6c). In addition, when we immunostained for subunits of the two retromer subcomplexes and compared their pattern with that of internalized pIgA, we saw a significant decrease in colocalization for both Vps26 (Fig. 8) and SNX2 (Fig. 9) when PI3K was inhibited. A reduction in colocalization was still observed even under Vps35 overexpression, in agreement with the observation that pIgA transcytosis in Vps35 overexpressing cells is still reduced by PI3K inhibition (Fig. 3b). A comparable analysis in MDCK-pIgR$^{\Delta 670\text{-}707}$ cells could not be performed because the low expression level of the mutant receptor, along with its faster turnover in comparison to pIgR-WT [9, 25], did not allow reliable detection of the internalized pIgA by immunofluorescence, even upon Vps35 overexpression. At any rate, we could conclude that, more precisely than simply a redistribution of SNXs to the cytosol, it seems clear that the primary effect of PI3K inhibition on SNXs is a loss of their proper membrane location due to reduction of PI 3-phosphates on membranes. In agreement with our results, data on the recently described plant retromer also shows that the Vps35-Vps26-Vps29

subcomplex remains membrane associated as a result of wortmannin treatment [50]. Although Vps5 staining could not be performed in that study, a loss of colocalization between Vps35 and cargo became evident by the treatment, indicative of a spatial redistribution of Vps35, Vps26, and Vps29 to different membrane subdomains [50]. In the absence of PI3K activity, it is therefore possible that the Vps35-Vps26-Vps29 subcomplex is still efficiently recruited to the membrane by means of an unrelated mechanism which, as recently suggested, might involve Vps26 interaction with an as yet unidentified transmembrane protein [19]. However, owed to its mislocalization with the SNXs subcomplex, it becomes unable to cluster the cargo for efficient sorting from appropriate locations, which must be defined by the SNXs subcomplex. This would provide an explanation to the effects on pIgA transcytosis that we see upon PI3K inhibition by LY294002.

In conclusion, we present evidence that PI3K regulates retromer's role in pIgR-pIgA transcytosis. Our data agree with the idea that retromer efficiently sorts pIgR-pIgA into the transcytotic pathway through interaction of pIgR with the Vps35-Vps26-Vps29 retromer subcomplex. While membrane association and assembly of the Vps35-Vps26-Vps29 subcomplex seems to proceed independently of SNXs association, proper functioning in sorting requires efficient membrane association of the SNXs subcomplex, which likely provides a site for the proper membrane location of the Vps35-Vps26-Vps29 subcomplex. Given the apparent independence of regulation between the two subcomplexes, an interesting challenge in the future will be to define whether different SNX family members interact with the Vps35-Vps26-Vps29 retromer subcomplex to perform specific sorting roles in mammalian systems.

Acknowledgements

Special thanks go to C. R. Haft for providing us with the cDNA constructs for expression of human Vps35 and SNX2, and for antibodies against retromer subunits. We also thank Maravillas Mellado for technical support. This investigation was supported by NIH grants to K. E. Mostov and a grant to M. Vergés from the Ministerio de Sanidad y Consumo (PI 04 / 1113), Spain. M. Vergés is recipient of a "Ramón y Cajal" contract by the Ministerio de Educación y Ciencia, Spain.

Figure legends

Figure 1 Effect of PI3K inhibition on Akt dephosphorylation and EEA1 membrane depletion. MDCK cells growing on plates were incubated with the indicated concentration of LY294002 (LY). Membrane (mem) and cytosolic (cyt) fractions were prepared from cell homogenates and analyzed by western blot. **a**, Dephosphorylation of cytosolic P-AKT at increasing concentrations of LY294002. The percentage of P-AKT dephosphorylation (% de-P) is indicated. **b,** EEA1 redistribution to cytosol by LY294002 (upper panel), with values below the panel showing percentage of membrane depletion (% depl). Actin, with a constant cytosol / membrane ratio (9:1), is included as a loading control (lower panel). Each lane was loaded with the same amount of protein (**a,** 20 μg; **b,** 10 μg).

Figure 2 Effect of PI3K inhibition on endosome size. MDCK cells were grown as a polarized monolayer on Transwells and treated with the indicated concentration of LY294002 (LY). Cells were fixed with paraformaldehyde and immunostained for EEA1. **a,** XY sections taken at high magnification, with arrowheads pointing to large endosomes seen using 100 μM

LY294002, some of them appearing blurry (asterisks). Scale bar represents 5 μm. **b,** Graph showing mean endosome size ± SD (number of endosomes, n ~ 350; *** $p < 0.0001$ vs. 0 μM).

Figure 3 PI3K inhibition reduces pIgA transcytosis with or without Vps35 overexpression. MDCK cells expressing pIgR-WT and the tetracycline transactivator (tTA) were grown as a polarized monolayer on Transwells and infected with adenovirus carrying the myc-hVps35 gene under a tetracycline repressible system. A ligand transcytosis assay using ^{125}I-pIgA was performed. **a,** Decrease of apically transcytosed ligand and concomitant increase in degradation in uninduced control cells (repressed with the antibiotic) treated with 50 μM LY294002 (50 μM), with little change when a lower concentration of inhibitor (10 μM) was used. **b,** Decrease of apically transcytosed ligand and slight increase in degradation in cells overexpressing ~ 5-fold Vps35 (adenoviral-induced) treated with increasing concentrations of LY294002. Apical delivery is represented by a solid line and degradation by a dashed line. Values are the mean ± SD (n = 3).

Figure 4 Vps35 overexpression does not restore pIgA transcytosis if PI3K is inhibited in MDCK-pIgR$^{\Delta 670\text{-}707}$ cells. MDCK cells expressing pIgR$^{\Delta 670\text{-}707}$ were grown as a polarized monolayer on Transwells and infected with adenovirus carrying the myc-hVps35 gene together with an adenovirus carrying the tTA under a tetracycline repressible system (co-infection was required because these cells do not stably express tTA). A ligand transcytosis assay using ^{125}I-pIgA was performed on cells treated (+ LY) or untreated (- LY) with 50 μM LY294002. **a,** LY294002 treatment in cells overexpressing ~ 5-fold Vps35 (adenoviral-induced) abolished apical transcytosis restored by Vps35 overexpression. In the presence of the inhibitor, uninduced control cells (repressed with the antibiotic) showed no change on

transcytosis, which remained at background levels. **b,** PI3K inhibition substantially increased basolateral recycling in uninduced cells and to a lesser extent in Vps35 overexpressing cells. **c,** PI3K inhibition reduced ligand degradation only in uninduced cells. The curves for uninduced cells are represented by a solid line and circles are used as symbols. For Vps35 overexpressing cells, the curves are dashed lines and diamonds are used as symbols. LY294002 treatment is denoted by filled symbols vs. empty symbols in untreated cells. Values are the mean ± SD (n = 3).

Figure 5 PI3K inhibition reduces membrane association of SNX1 and SNX2 but does not affect the Vps35-Vps26-Vps29 subcomplex. MDCK cells were treated with 0 μM or 50 μM LY294002 (LY) and processed for subcellular fractionation and western blot analysis as in Fig. 1. **a,** To better visualize possible redistribution between the fractions, 10 μg cytosol (cyt) and 20 μg membrane (mem) protein were loaded, except for the blot to Vps35 shown, which was loaded with 20 μg cytosol and 10 μg membrane protein. A considerable redistribution to cytosol of SNX1 and SNX2 is observed using 50 μM LY294002, leaving Vps35, Vps26 and Vps29 unaffected. **b,** Graph showing percentage of membrane association for the retromer subunits using various concentrations of LY294002 as obtained by quantitation of 3-5 western blots. Values are the mean ± S.E. (* $p < 0.05$; ** $p < 0.005$ vs. 0 μM).

Figure 6 Co-immunoprecipitation of Vps35-Vps26-Vps29 is not affected by PI3K inhibition but association of Vps35 with pIgR is reduced. MDCK cells growing on plates were lysed with non-ionic detergent and subjected to Vps26 (**a-b**) or pIgR (**c**) immunoprecipitation (IP). Western blot analysis shows co-immunoprecipitated proteins. **a,** 28.6 ± 5.5 % Vps35 and 76.9 ± 10.9 % Vps29 (mean ± SD; n = 8) were found complexed

with Vps26, while SNX1 or SNX2 were not detected in the immunoprecipitates. The lane with antibody alone (no lysate; Blk) indicates the bands originated from the antibody IgG. For clarity, exposure time is lower in blots for Vps35, Vps26 and Vps29 shown in the IP lanes than in those of the lysate lane. **b,** No change in the relative association among the subunits of the Vps35-Vps26-Vps29 subcomplex upon treatment with 50 μM LY294002. The anti-Vps26 antibody used here was chemically cross-linked to protein A-Sepharose beads. **c,** Less Vps35 associates with pIgR in LY294002 treated cells (0.66 ± 0.39 %; mean ± S.E.; n = 6; $p < 0.05$ vs. 0 μM) in comparison to untreated cells (1.73 ± 0.29 %). Lysates (Lys), 15 μg protein. Immunoprecipitations were from ~ 750 μg protein as starting material.

Figure 7 PI3K inhibition reduces colocalization between the two retromer subcomplexes. MDCK cells expressing myc-SNX2 were grown as a polarized monolayer on Transwells. After treatment with 0 μM or 50 μM LY294002, cells were fixed with paraformaldehyde and immunostained for Vps26 (green) and myc (red). **a,** XY sections taken at the subapical cell region show a single enlarged cell. Vps26 is distributed in this region in structures of various sizes displaying evident colocalization with myc-SNX2 (arrowheads), which was reduced upon treatment with LY294002. Scale bar represents 2.5 μm. **b,** The graph shows percentage of myc-SNX2 colocalizing with Vps26 throughout three representative cell levels, subapical (API), medial or nuclear level (NUC), and basolateral region (BAS); a general loss of colocalization was seen upon treatment with the inhibitor. Values are the mean ± S.E. (number of structures, n ~ 80; ** $p < 0.005$; *** $p < 0.0005$ vs. 0 μM).

Figure 8 PI3K inhibition reduces colocalization between Vps26 and internalized pIgA with or without Vps35 overexpression. MDCK cells expressing pIgR-WT and the tetracycline transactivator (tTA) were grown as a polarized monolayer on Transwells and

infected with adenovirus carrying the myc-hVps35 gene under a tetracycline repressible system. After pretreatment with 0 μM or 50 μM LY294002, pIgA was internalized from the basolateral cell pole for 10 min at 37°C, and then chased for 2.5 min in ligand-free medium. Cells were fixed with paraformaldehyde and immunostained for Vps26 (green) and pIgA (red). **a,** XY sections taken at the level of the nucleus show a single enlarged cell (uninduced control, repressed with the antibiotic). Vps26 is distributed in this region in structures of various sizes displaying considerable colocalization with pIgA (arrowheads), which was reduced upon treatment with LY294002. Scale bar represents 2.5 μm. **b-c,** The graphs show percentage of pIgA colocalizing with Vps26 throughout three representative cell levels, as in Fig. 7. Upon treatment with the inhibitor, a general loss of colocalization was seen either in uninduced (**b**) or in adenoviral induced cells (overexpressing Vps35; **c**). Values are the mean ± S.E. (number of structures, n ~ 80; * $p < 0.05$; ** $p < 0.005$; *** $p < 0.0005$ vs. 0 μM).

Figure 9 PI3K inhibition reduces colocalization between SNX2 and internalized pIgA with or without Vps35 overexpression. MDCK cells expressing pIgR-WT and the tetracycline transactivator (tTA) were grown as a polarized monolayer on Transwells and treated as described in Fig. 8. After fixation, cells were immunostained for SNX2 (green) and pIgA (red). **a,** XY sections taken at the subapical cell region show a single enlarged cell (uninduced control, repressed with the antibiotic). SNX2 is distributed in this region in structures of various sizes displaying visible colocalization with pIgA (arrowheads), which was reduced upon treatment with LY294002. Scale bar represents 2.5 μm. **b-c,** The graphs show percentage of pIgA colocalizing with SNX2 throughout three representative cell levels, as in Fig. 7. Upon treatment with the inhibitor, a general loss of colocalization was seen either in uninduced (**b**) or in adenoviral induced cells (overexpressing Vps35; **c**). Values are the mean ± S.E. (number of structures, n ~ 80; ** $p < 0.005$; *** $p < 0.0005$ vs. 0 μM).

Supplemental Figure 1 PI3K inhibition reduces colocalization between Vps26 and internalized pIgA chased for a long time period. MDCK cells expressing pIgR-WT were grown as a polarized monolayer on Transwells. Cells were treated with 0 μM or 50 μM LY294002 and processed for immunofluorescence as in Fig. 8, except that here internalized pIgA was chased for 2.5, 10, 15 or 30 min, as indicated. **a-c,** The graphs show percentage of pIgA colocalizing with Vps26 throughout three representative cell levels, as in Fig. 7; a general loss of colocalization at the different chase times was seen upon treatment with LY294002 (number of structures, n ~ 80; * $p < 0.05$; ** $p < 0.005$; *** $p < 0.0005$ vs. 0 μM).

Supplemental Figure 2 PI3K inhibition reduces colocalization between SNX2 and internalized pIgA chased for a long time period. MDCºK cells expressing pIgR-WT were grown as a polarized monolayer on Transwells. Cells were treated with 0 μM or 50 μM LY294002 and processed for immunofluorescence as in Fig. 9, except that here internalized pIgA was chased for 2.5, 10, 15 or 30 min, as indicated. **a-c,** The graphs show percentage of pIgA colocalizing with SNX2 throughout three representative cell levels, as in Fig. 7; a general loss of colocalization at the different chase times was seen upon treatment with LY294002. Values are the mean ± S.E. (number of structures, n ~ 80; * $p < 0.05$; *** $p < 0.0005$ vs. 0 μM).

References

1. K. Mostov, T. Su, M. ter Beest, Polarized epithelial membrane traffic: conservation and plasticity, Nat. Cell Biol. 5 (2003) 287-293.

2. P.L. Tuma, A.L. Hubbard, Transcytosis: crossing cellular barriers, Physiol. Rev. 83 (2003) 871-932.

3. R. Rojas, G. Apodaca, Immunoglobulin transport across polarized epithelial cells, Nature Rev. Mol. Cell Biol. 3 (2002) 944-956.

4. M.N. Seaman, J.M. McCaffery, S.D. Emr, A membrane coat complex essential for endosome-to-Golgi retrograde transport in yeast, J. Cell Biol. 142 (1998) 665-681.

5. M.N. Seaman, E.G. Marcusson, J.L. Cereghino, S.D. Emr, Endosome to Golgi retrieval of the vacuolar protein sorting receptor, Vps10p, requires the function of the VPS29, VPS30, and VPS35 gene products, J. Cell Biol. 137 (1997) 79-92.

6. C.N. Arighi, L.M. Hartnell, R.C. Aguilar, C.R. Haft, J.S. Bonifacino, Role of the mammalian retromer in sorting of the cation-independent mannose 6-phosphate receptor, J. Cell Biol. 165 (2004) 123-133.

7. M.N. Seaman, Cargo-selective endosomal sorting for retrieval to the Golgi requires retromer, J. Cell Biol. 165 (2004) 111-122.

8. M.N. Seaman, Recycle your receptors with retromer, Trends Cell Biol. 15 (2005) 68-75.

9. M. Vergés, F. Luton, C. Gruber, F. Tiemann, L.G. Reinders, L. Huang, A.L. Burlingame, C.R. Haft, K.E. Mostov, The mammalian retromer regulates transcytosis of the polymeric immunoglobulin receptor, Nat. Cell Biol. 6 (2004) 763-739.

10. J.S. Bonifacino, R. Rojas, Retrograde transport from endosomes to the trans-Golgi network, Nat. Rev. Mol. Cell Biol. 7 (2006) 568-579.

11. M.N. Seaman, H.P. Williams, Identification of the functional domains of yeast sorting nexins Vps5p and Vps17p, Mol. Biol. Cell 13 (2002) 2826-2840.

12. B.F. Horazdovsky, B.A. Davies, M.N. Seaman, S.A. McLaughlin, S. Yoon, S.D. Emr, A sorting nexin-1 homologue, Vps5p, forms a complex with Vps17p and is required for recycling the vacuolar protein-sorting receptor, Mol. Biol. Cell 8 (1997) 1529-1541.

13. S.F. Nothwehr, P. Bruinsma, L.A. Strawn, Distinct domains within Vps35p mediate the retrieval of two different cargo proteins from the yeast prevacuolar/endosomal compartment, Mol. Biol. Cell 10 (1999) 875-890.

14. S.F. Nothwehr, S.A. Ha, P. Bruinsma, Sorting of yeast membrane proteins into an endosome-to-Golgi pathway involves direct interaction of their cytosolic domains with Vps35p, J. Cell Biol. 151 (2000) 297-310.

15. J.V. Reddy, M.N. Seaman, Vps26p, a component of retromer, directs the interactions of Vps35p in endosome-to-Golgi retrieval, Mol. Biol. Cell 12 (2001) 3242-3256.

16. C.R. Haft, M. de la Luz Sierra, R. Bafford, M.A. Lesniak, V.A. Barr, S.I. Taylor, Human orthologs of yeast vacuolar protein sorting proteins Vps26, 29, and 35: assembly into multimeric complexes, Mol. Biol. Cell 11 (2000) 4105-4116.

17. B.M. Collins, C.F. Skinner, P.J. Watson, M.N. Seaman, D.J. Owen, Vps29 has a phosphoesterase fold that acts as a protein interaction scaffold for retromer assembly, Nat. Struct. Mol. Biol. 12 (2005) 594-602.

18. D. Wang, M. Guo, Z. Liang, J. Fan, Z. Zhu, J. Zang, X. Li, M. Teng, L. Niu, Y. Dong, P. Liu, Crystal structure of human vacuolar protein sorting protein 29 reveals a

phosphodiesterase/nuclease-like fold and two protein-protein interaction sites, J. Biol. Chem. 280 (2005) 22962-22967.

19. H. Shi, R. Rojas, J.S. Bonifacino, J.H. Hurley, The retromer subunit Vps26 has an arrestin fold and binds Vps35 through its C-terminal domain, Nat. Struct. Mol. Biol. 13 (2006) 540-548.

20. P. Burda, S.M. Padilla, S. Sarkar, S.D. Emr, Retromer function in endosome-to-Golgi retrograde transport is regulated by the yeast Vps34 PtdIns 3-kinase, J. Cell Sci. 115 (2002) 3889-3900.

21. Q. Zhong, C.S. Lazar, H. Tronchere, T. Sato, T. Meerloo, M. Yeo, Z. Songyang, S.D. Emr, G.N. Gill, Endosomal localization and function of sorting nexin 1, Proc. Natl. Acad. Sci. U S A 99 (2002) 6767-6772.

22. S.H. Hansen, A. Olsson, J.E. Casanova, Wortmannin, an inhibitor of phosphoinositide 3-kinase, inhibits transcytosis in polarized epithelial cells, J. Biol. Chem. 270 (1995) 28425-28432.

23. M. Cardone, K. Mostov, Wortmannin inhibits transcytosis of dimeric IgA by the polymeric immunoglobulin receptor, FEBS Lett. 376 (1995) 74-76.

24. A.I. Barth, A.L. Pollack, Y. Altschuler, K.E. Mostov, W.J. Nelson, NH2-terminal deletion of beta-catenin results in stable colocalization of mutant beta-catenin with adenomatous polyposis coli protein and altered MDCK cell adhesion, J. Cell Biol. 136 (1997) 693-706.

25. P.P. Breitfeld, J.E. Casanova, W.C. McKinnon, K.E. Mostov, Deletions in the cytoplasmic domain of the polymeric immunoglobulin receptor differentially affect endocytotic rate and postendocytotic traffic, J. Biol. Chem. 265 (1990) 13750-13757.

26. K.L. Singer, K.E. Mostov, Dimerization of the polymeric immunoglobulin receptor controls its transcytotic trafficking, Mol. Biol. Cell 9 (1998) 901-915.

27. F. Luton, M.H. Cardone, M. Zhang, K.E. Mostov, Role of tyrosine phosphorylation in ligand-induced regulation of transcytosis of the polymeric Ig receptor, Mol. Biol. Cell 9 (1998) 1787-1802.

28. C.J. Vlahos, W.F. Matter, K.Y. Hui, R.F. Brown, A specific inhibitor of phosphatidylinositol 3-kinase, 2-(4-morpholinyl)-8-phenyl-4H-1-benzopyran-4-one (LY294002), J. Biol. Chem. 269 (1994) 5241-5248.

29. L.C. Cantley, The phosphoinositide 3-kinase pathway, Science 296 (2002) 1655-1657.

30. V. Patki, J. Virbasius, W.S. Lane, B.H. Toh, H.S. Shpetner, S. Corvera, Identification of an early endosomal protein regulated by phosphatidylinositol 3-kinase, Proc. Natl. Acad. Sci. U S A 94 (1997) 7326-7330.

31. X. Chen, Z. Wang, Regulation of epidermal growth factor receptor endocytosis by wortmannin through activation of Rab5 rather than inhibition of phosphatidylinositol 3-kinase, EMBO Rep. 2 (2001) 842-849.

32. P.L. Tuma, C.M. Finnegan, J.H. Yi, A.L. Hubbard, Evidence for apical endocytosis in polarized hepatic cells: phosphoinositide 3-kinase inhibitors lead to the lysosomal accumulation of resident apical plasma membrane proteins, J. Cell Biol. 145 (1999) 1089-1102.

mediating brefeldin A-sensitive basolateral targeting from the trans-Golgi network, J. Biol. Chem. 274 (1999) 2201-2215.

41. E.H. Walker, M.E. Pacold, O. Perisic, L. Stephens, P.T. Hawkins, M.P. Wymann, R.L. Williams, Structural determinants of phosphoinositide 3-kinase inhibition by wortmannin, LY294002, quercetin, myricetin, and staurosporine, Mol. Cell 6 (2000) 909-919.

42. H. Shpetner, M. Joly, D. Hartley, S. Corvera, Potential sites of PI-3 kinase function in the endocytic pathway revealed by the PI-3 kinase inhibitor, wortmannin, J. Cell Biol. 132 (1996) 595-605.

43. C.A. Worby, J.E. Dixon, Sorting out the cellular functions of sorting nexins, Nature Rev. Mol. Cell Biol. 3 (2002) 919-931.

44. J. Carlton, M. Bujny, A. Rutherford, P. Cullen, Sorting nexins-unifying trends and new perspectives, Traffic 6 (2005) 75-82.

45. L.F. Seet, W. Hong, The Phox (PX) domain proteins and membrane traffic, Biochim. Biophys. Acta 1761 (2006) 878-896.

46. J.H. Stack, D.B. DeWald, K. Takegawa, S.D. Emr, Vesicle-mediated protein transport: regulatory interactions between the Vps15 protein kinase and the Vps34 PtdIns 3-kinase essential for protein sorting to the vacuole in yeast, J. Cell Biol. 129 (1995) 321-334.

47. J. Carlton, M. Bujny, B.J. Peter, V.M. Oorschot, A. Rutherford, H. Mellor, J. Klumperman, H.T. McMahon, P.J. Cullen, Sorting nexin-1 mediates tubular endosome-to-TGN transport through coincidence sensing of high- curvature membranes and 3-phosphoinositides, Curr. Biol. 14 (2004) 1791-1800.

33. C.E. Futter, L.M. Collinson, J.M. Backer, C.R. Hopkins, Human VPS34 is required for internal vesicle formation within multivesicular endosomes, J. Cell Biol. 155 (2001) 1251-1264.

34. S. Christoforidis, H.M. McBride, R.D. Burgoyne, M. Zerial, The Rab5 effector EEA1 is a core component of endosome docking, Nature 397 (1999) 621-625.

35. H.W. Davidson, Wortmannin causes mistargeting of procathepsin D. Evidence for the involvement of a phosphatidylinositol 3-kinase in vesicular transport to lysosomes, J. Cell Biol. 130 (1995) 797-805.

36. W.J. Brown, D.B. DeWald, S.D. Emr, H. Plutner, W.E. Balch, Role for phosphatidylinositol 3-kinase in the sorting and transport of newly synthesized lysosomal enzymes in mammalian cells, J. Cell Biol. 130 (1995) 781-796.

37. G. Apodaca, L.A. Katz, K.E. Mostov, Receptor-mediated transcytosis of IgA in MDCK cells is via apical recycling endosomes, J. Cell Biol. 125 (1994) 67-86.

38. G.J. Brunn, J. Williams, C. Sabers, G. Wiederrecht, J.C. Lawrence, Jr., R.T. Abraham, Direct inhibition of the signaling functions of the mammalian target of rapamycin by the phosphoinositide 3-kinase inhibitors, wortmannin and LY294002, Embo J. 15 (1996) 5256-5267.

39. S.P. Davies, H. Reddy, M. Caivano, P. Cohen, Specificity and mechanism of action of some commonly used protein kinase inhibitors, Biochem. J. 351 (2000) 95-105.

40. E. Orzech, K. Schlessinger, A. Weiss, C.T. Okamoto, B. Aroeti, Interactions of the AP-1 Golgi adaptor with the polymeric immunoglobulin receptor and their possible role in

48. J.G. Carlton, M.V. Bujny, B.J. Peter, V.M. Oorschot, A. Rutherford, R.S. Arkell, J. Klumperman, H.T. McMahon, P.J. Cullen, Sorting nexin-2 is associated with tubular elements of the early endosome, but is not essential for retromer-mediated endosome-to-TGN transport, J. Cell Sci. 118 (2005) 4527-4539.

49. A. Gullapalli, B.L. Wolfe, C.T. Griffin, T. Magnuson, J. Trejo, An Essential Role for SNX1 in Lysosomal Sorting of Protease-activated Receptor-1: Evidence for Retromer-, Hrs-, and Tsg101-independent Functions of Sorting Nexins, Mol. Biol. Cell 17 (2006) 1228-1238.

50. P. Oliviusson, O. Heinzerling, S. Hillmer, G. Hinz, Y.C. Tse, L. Jiang, D.G. Robinson, Plant retromer, localized to the prevacuolar compartment and microvesicles in Arabidopsis, may interact with vacuolar sorting receptors, Plant Cell 18 (2006) 1239-1252.

a

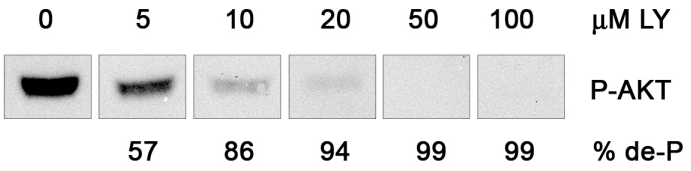

b

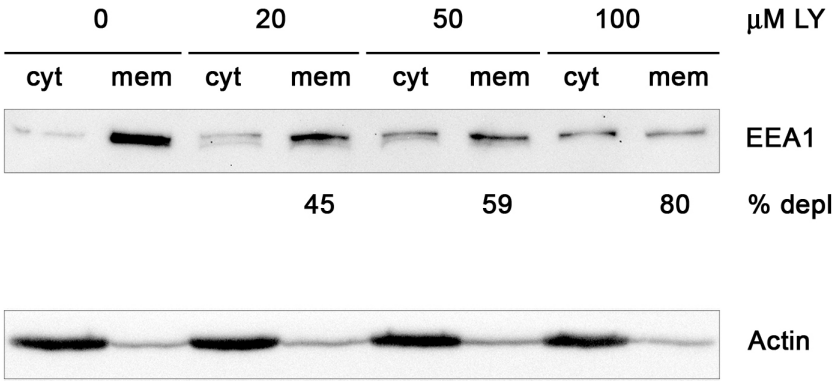

Figure 1 ECR-06-485

a

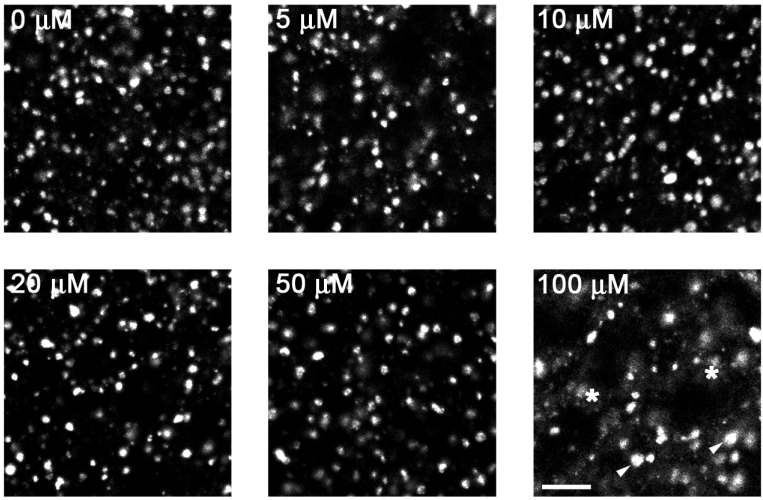

b

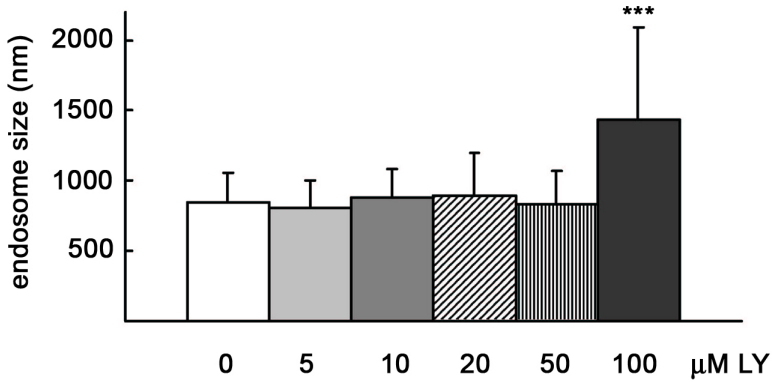

Figure 2 ECR-06-485

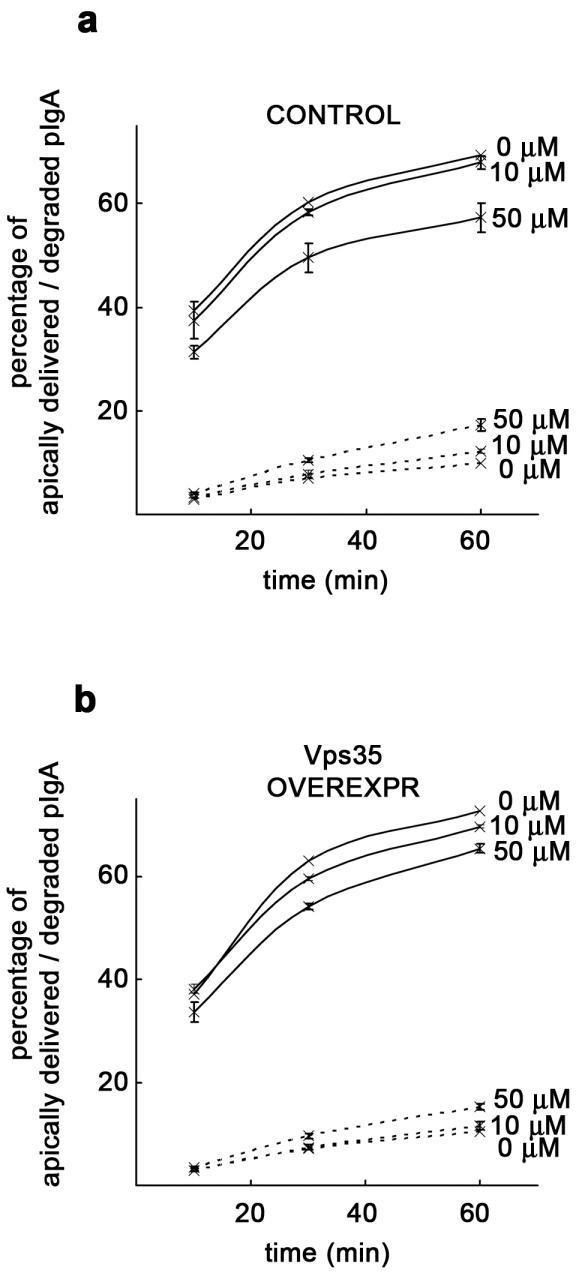

Figure 3 ECR-06-485

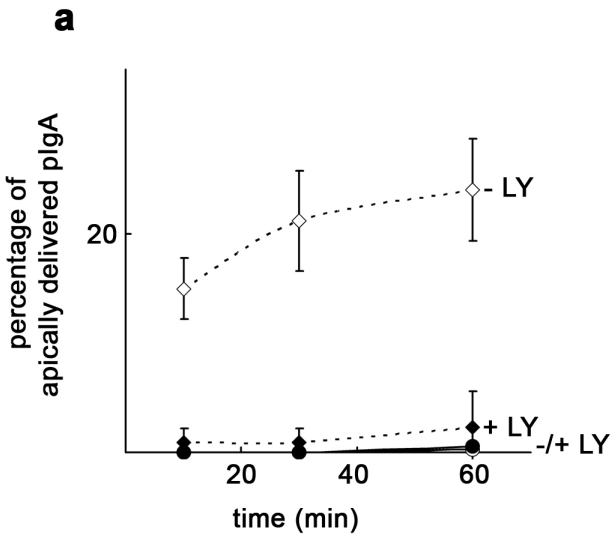

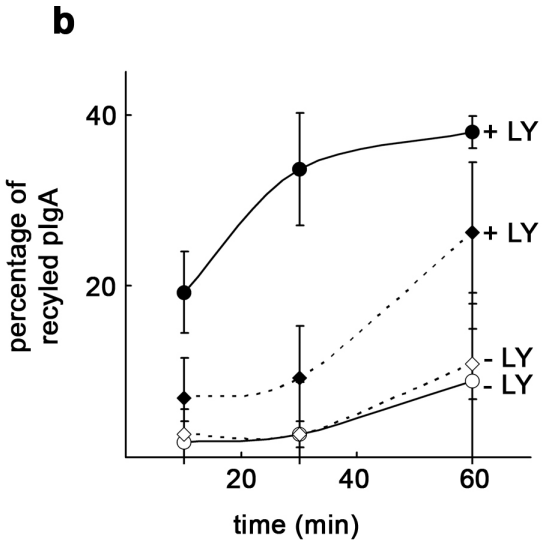

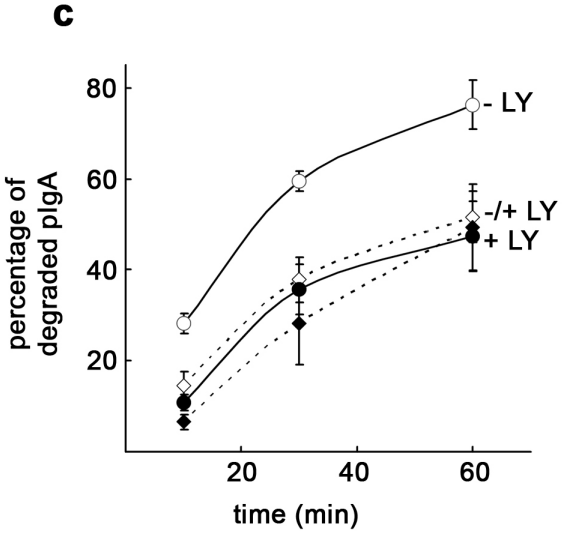

Figure 4 ECR-06-485

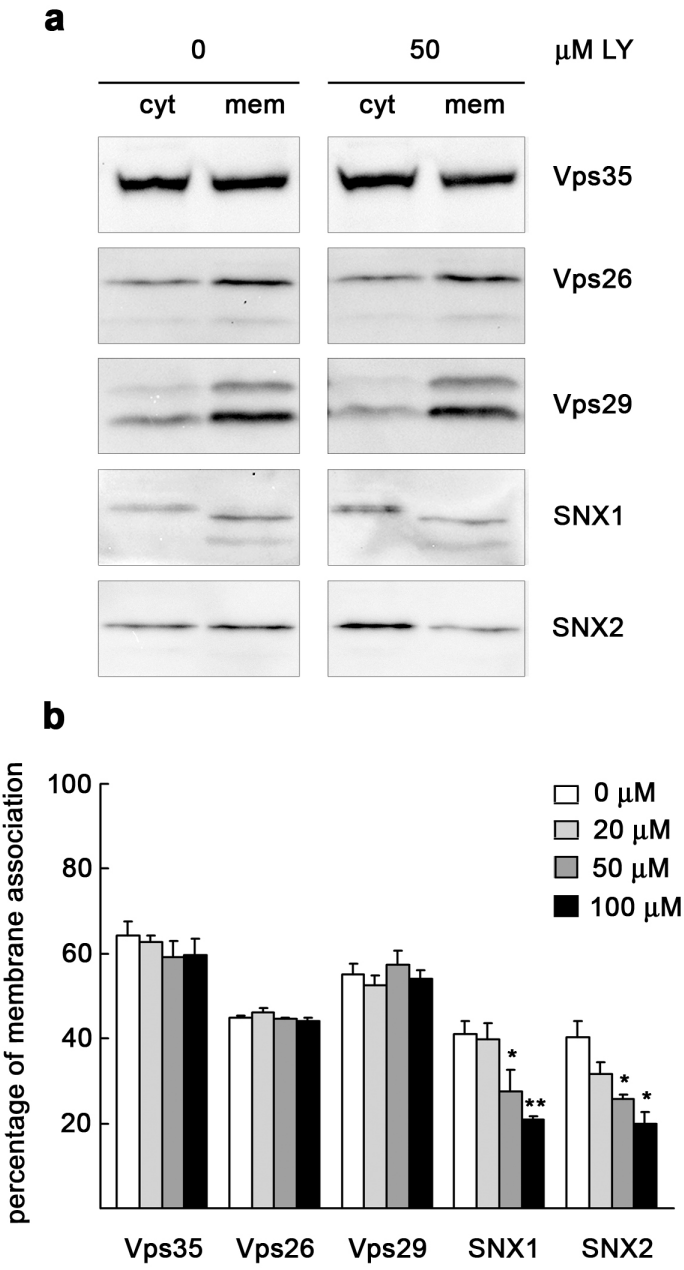

Figure 5 ECR-06-485

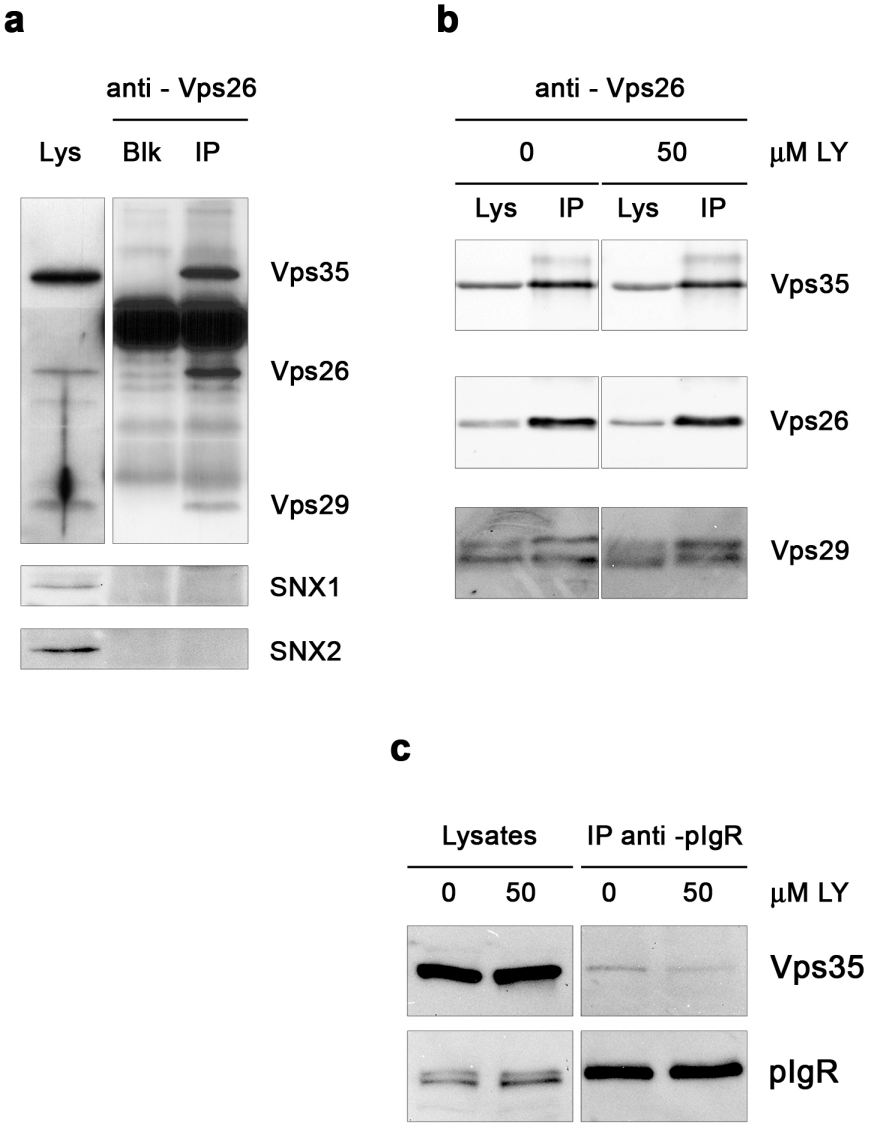

Figure 6 ECR-06-485

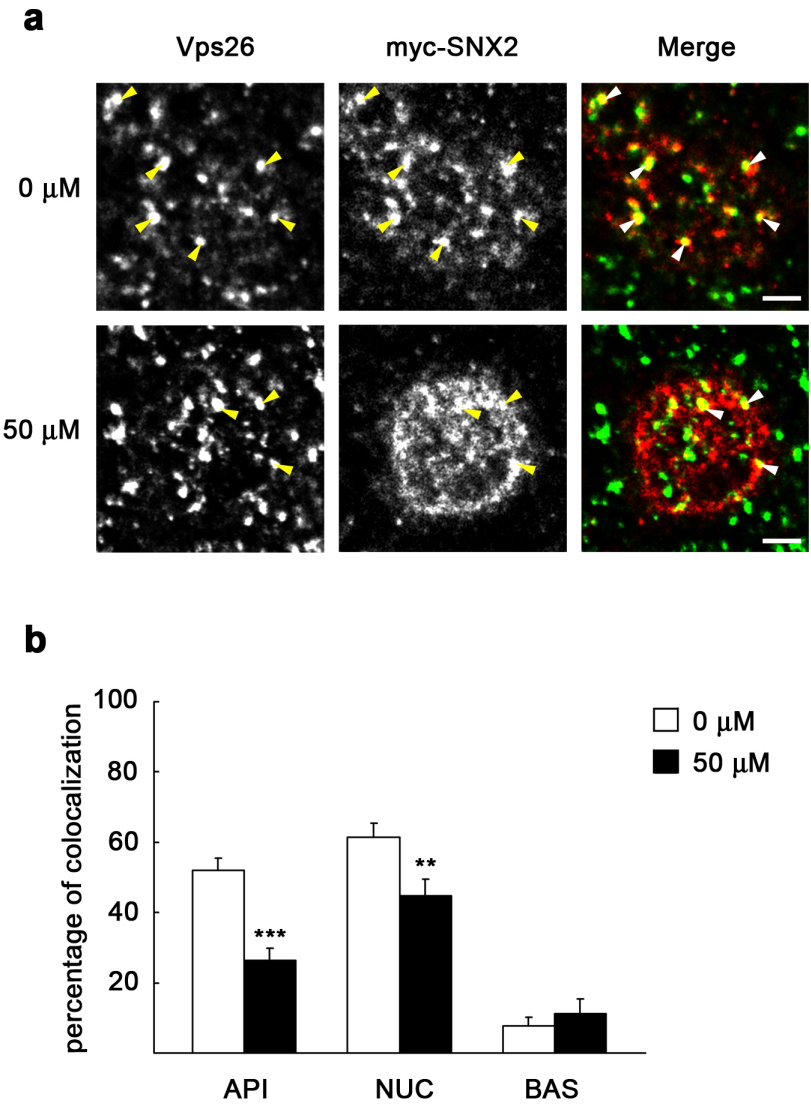

Figure 7 ECR-06-485

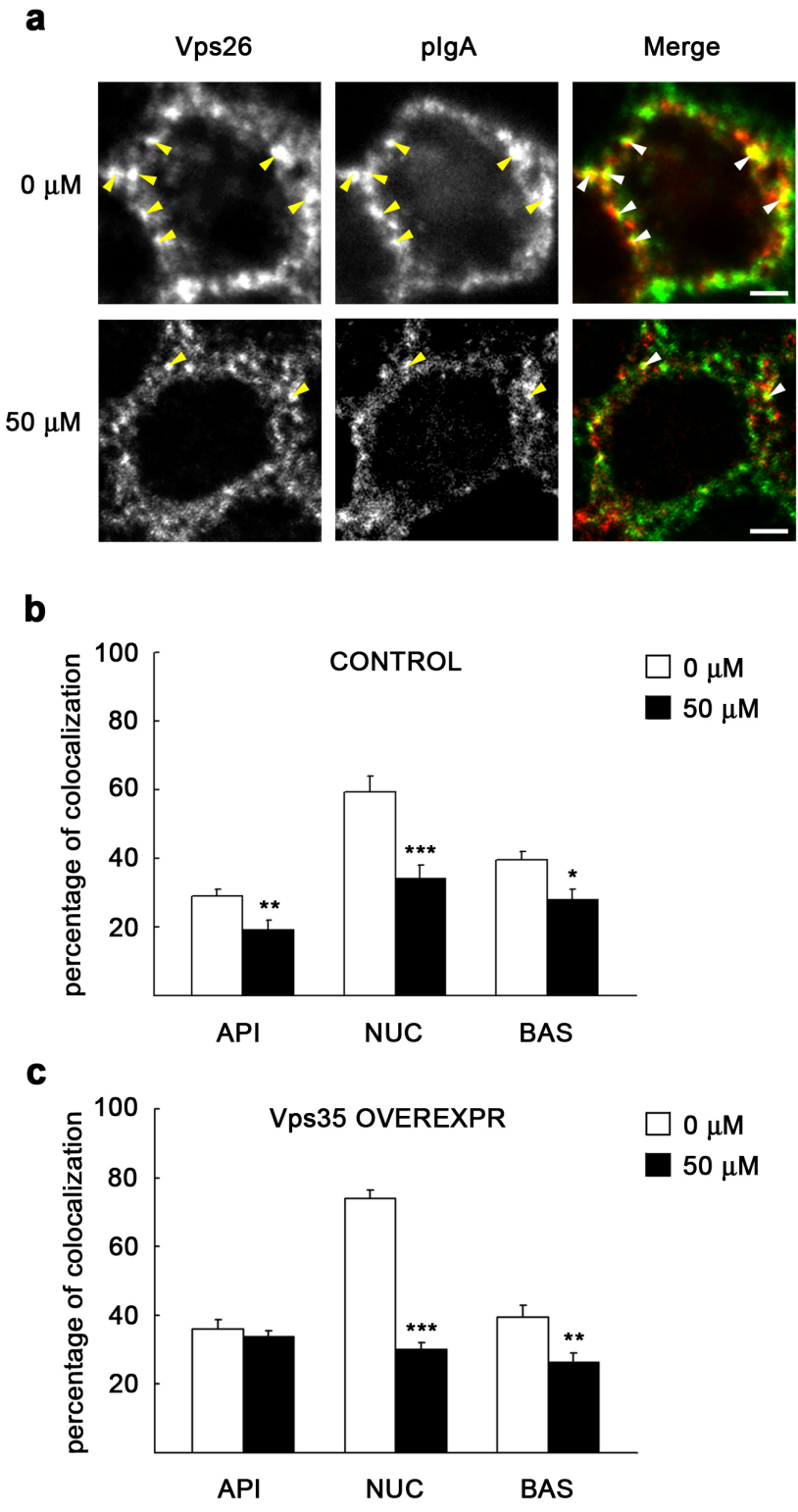

Figure 8 ECR-06-485

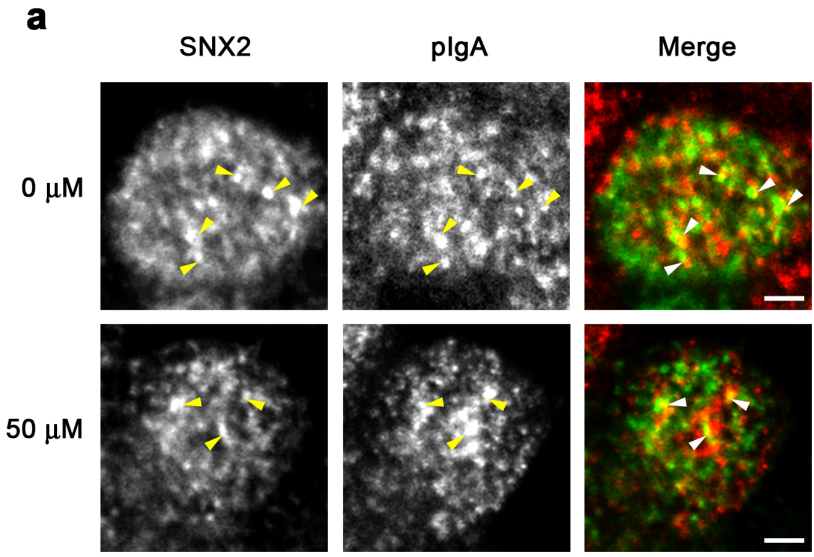

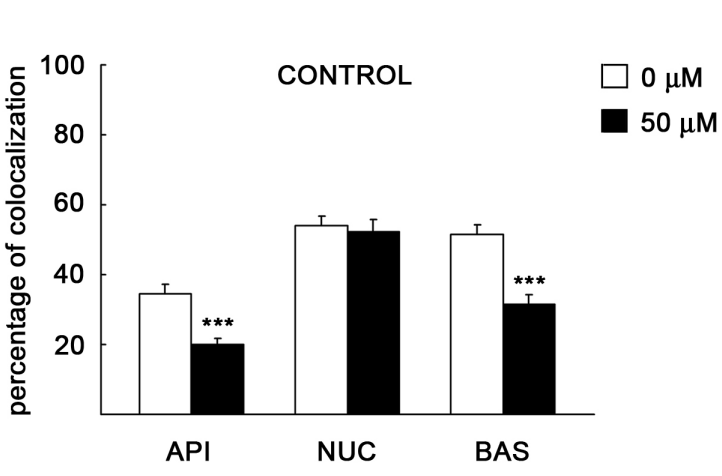

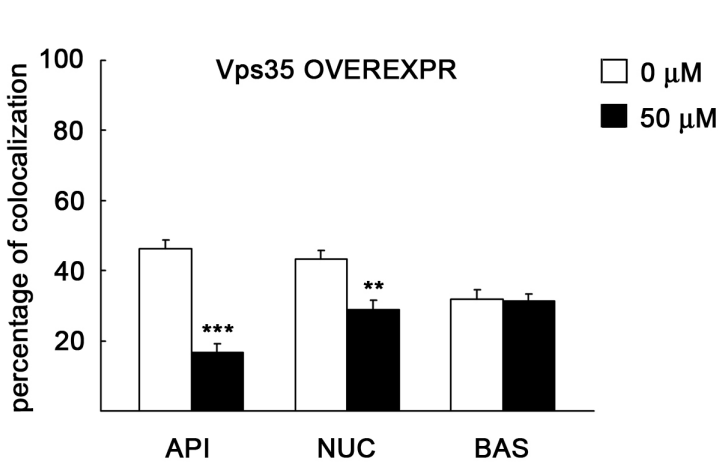

Figure 9-ECR-06-485

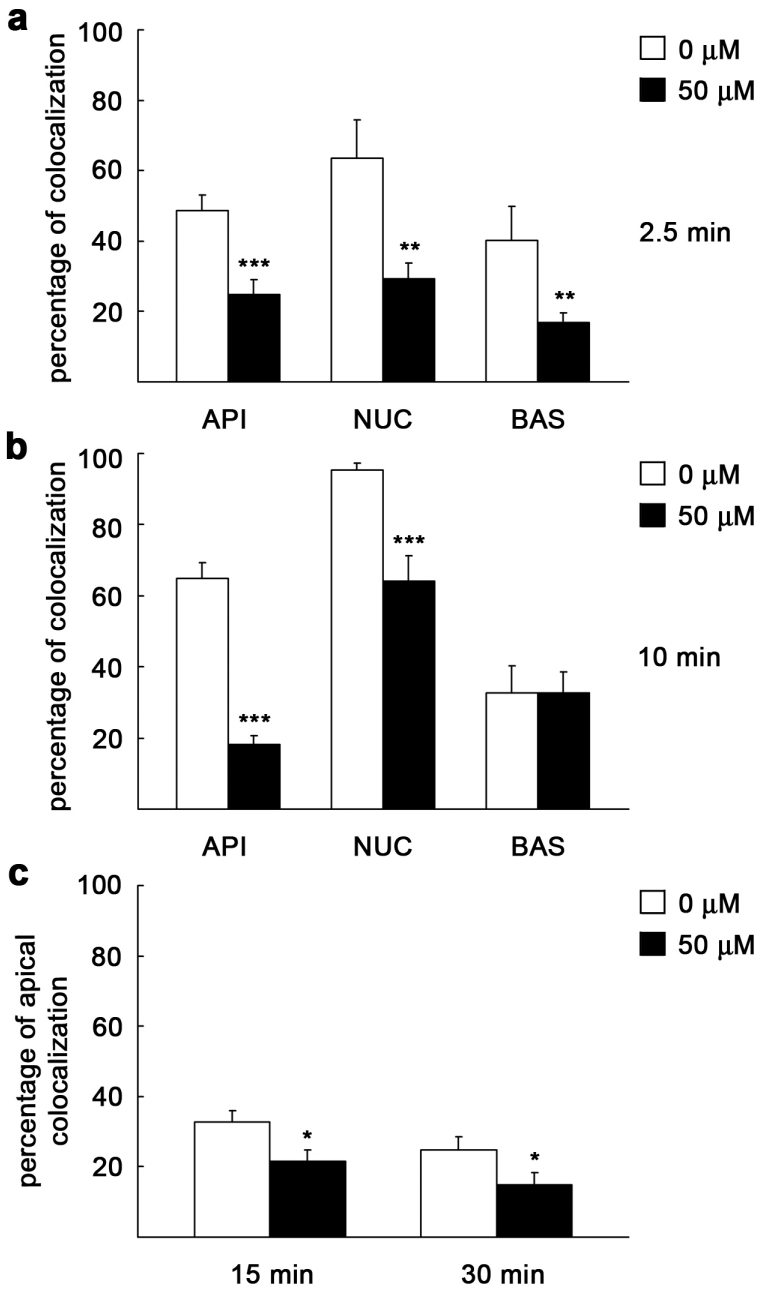

Suppl. Figure 1 ECR-06-485

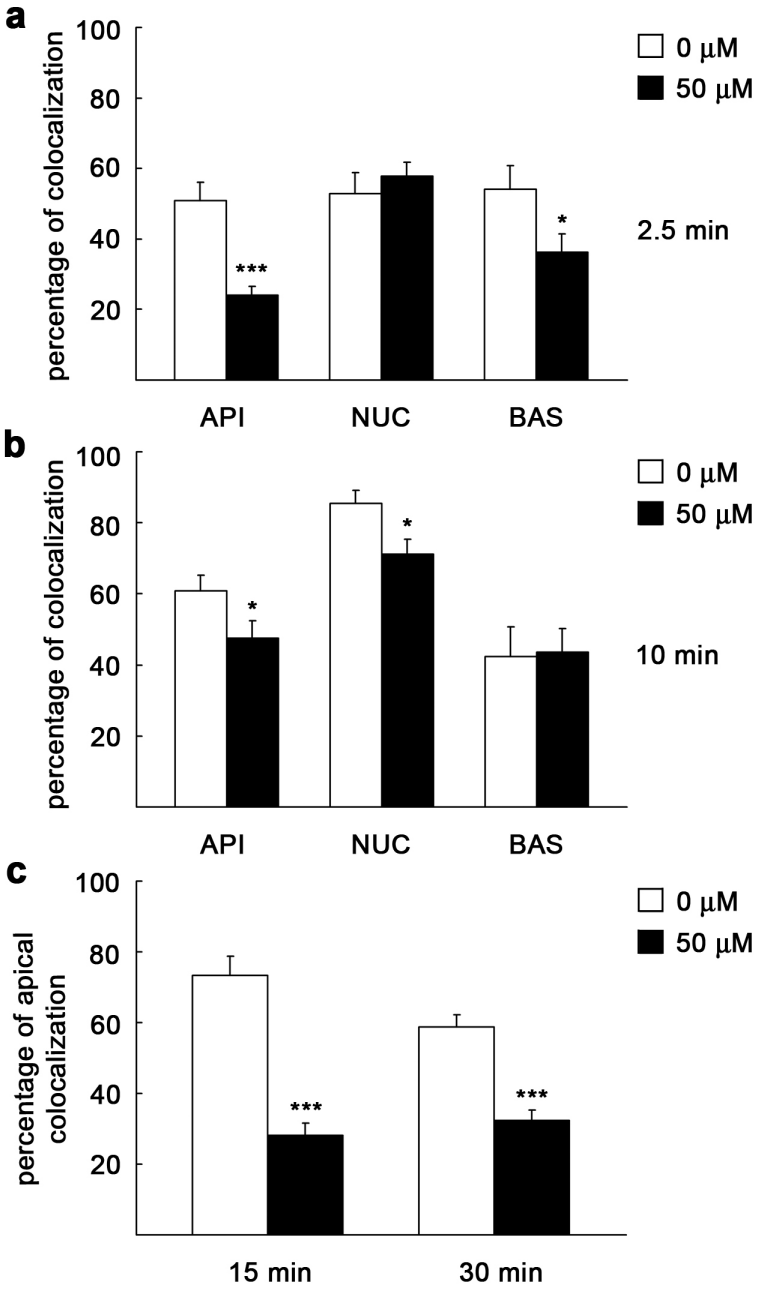

Suppl. Figure 2 ECR-06-485